IEEE Access
Multidisciplinary | Rapid Review | Open Access Journal

Received September 12, 2019, accepted October 4, 2019, date of publication October 8, 2019, date of current version October 21, 2019.

Digital Object Identifier 10.1109/ACCESS.2019.2946183

New Fault Tolerance Method for Open-Phase PMSM

XINXIU ZHOU[1], (Member, IEEE), SHUN LI[1], MING LU[2], FANQUAN ZENG[3], MIN ZHU[4], AND YANG YU[5]

[1]Fundamental Science on Novel Inertial Instrument and Navigation System Technology Laboratory, Beihang University, Beijing 100191, China
[2]Beijing Institute of Control Engineering, Beijing 100190, China
[3]Shanghai Institute of Spaceflight Control Technology, Shanghai 201109, China
[4]Shanghai Institute of Satellite Engineering, Shanghai 201109, China
[5]Centre for Built Infrastructure Research, Faculty of Engineering and IT, University of Technology Sydney, Sydney, NSW 2007, Australia

Corresponding author: Shun Li (lishun27@sina.com)

This work was supported in part by the National Natural Science Foundation of China under Grant 61873020, in part by the National Key Research and Development Program under Grant 2016YFB0500801 and Grant 2016YFB0500803, and in part by the Key Laboratory Fund of State Bureau of Surveying, Mapping, and Geographical Information under Grant KLSMTA-201709.

ABSTRACT Once the motor stator winding is opened, balanced three-phase windings turn into unbalanced two-phases windings. Unfortunately, by conducting Clarke and Park transformation for open-phase PMSM, complete decoupling of the torque and flux cannot achieve. To maintain the rated torque, the two remained phase currents have to be modified as sinusoidal currents with 60° phase difference (not 120°). As a result, the current controller design becomes complicated. In order to solve this problem, a new fault tolerance method for the open-phase PMSM is proposed in this paper. It is designed based on a novel reference frame transformation. Through proposed frame transformation, the modified sinusoidal time-varying current commands are turned into dc variables in the redefined synchronous rotating frame. Hence, the design of the open-phase PMSM current controller can be simplified. This method can deal with different phase open fault and different current control mode ($i_d = 0$ or $i_d \neq 0$ mode). In addition, considering that the neutral current ripple at usual switching frequencies may be very high, an optimal additional inductance that inserted into the neutral wire is designed. With the designed additional inductance, complete decoupling can be achieved. Experimental results confirm that the reliability and the performance of the PMSM drive can be improved distinctly with the proposed open-phase fault tolerance strategy.

INDEX TERMS Fault tolerance, open-phase motor, PMSM, reference frame transformation.

I. INTRODUCTION

Permanent magnet synchronous motor (PMSM) is attractive for a variety of applications owing to its high efficiency and power density. In some critical applications, such as spacecraft, aircraft, electric vehicles, motor drive system reliability is very important [1]. However, faults may present in motor winding or power converter, which mainly refer to short-circuit and open-circuit faults [2], [3]. Generally, the short-circuit fault can be dealt as open-circuit fault. Therefore, the open-circuit faults have received more attention in recent years [4]–[7].

When inverter open-fault occurs, three-phase inverter can be reconfigured by backup switch. However, backup winding is impracticable for most of industrial PMSM due to the increased complexity and volume. For the three-phase PMSM, only two phases windings remain under open-phase fault. If the traditional Clarke and Park transformations is employed, motor system equation would contain strong nonlinear. Complete decoupling of the motor torque and flux cannot be achieved, and the controller design becomes complicated under open-phase fault.

According to [8], [9], the performance of the open-phase PMSM can be preserved as long as the current in the remained two phases generate the same dq-axes current components as that in pre-fault state. It can be derived that to preserve same rated torque, the phase current amplitude should increase by $\sqrt{3}$ times, and the phase differences between the two remained phases should be regulated to 60°, no longer 120°. This implies that the PMSM current controllers are required

The associate editor coordinating the review of this manuscript and approving it for publication was Hao Luo.

to track two sinusoidal signals in A-B-C reference frame, whose frequency is motor rotation frequency and the phase differences are 60°. Obviously, the conventional PI current controllers are unsuitable to regulate this kind of sinusoidal currents, especially at high speed range.

In order to track the sinusoidal current commands in A-B-C reference frame, the hysteresis current controller is employed during open-phase motor operation in [10] and [11]. However, the system based on hysteresis controller suffers from the inconstant switch frequency, and the yielded tracking performance is restricted. Resonant controller provides infinite gain at its resonant frequency and can be employed to solve similar problems [12]. However, due to its high selectivity, its performance depends on the accuracy of the resonant frequency [13]. Inaccurate frequency may lead to significant loss of performance. If PR controller is employed during PMSM acceleration or deceleration, the sinusoidal current tracking performance would degrade under the existence of speed/parameter variations and back-EMF disturbance [14]–[16].

After that, A. Gaeta proposed a three-phase induction motor modeling and field-oriented control method under open-phase fault [17]. It is designed based on the three-leg inverter with the neutral wire connected to the middle point of a split capacitor. The voltage and current are decoupled by exploiting suitable reference frame transformations. However, the analysis and modeling of the open-phase induction motor presented in [17] are very complicated and it is not suitable for the PMSM fault-tolerant system with four-leg inverter [19]–[23].

Well known that the fault-tolerance of three-phase PMSM can be designed based on three-phase inverter [17], [24] or four-leg inverter [19]–[23]. The former topology is designated as extra-leg split capacitor that connected to the neutral point for reconfiguration after fault (ELSC for short). While in the latter topology, the neutral point is linked to the fourth inverter leg (ELES for short). K. D. Hoang analyzed the pros and cons of these two topologies in [25]. In the ELSC topology, motor maximum speed reduces to half of its nominal value since the applied voltage is decreased by half [25]. In addition, its voltage and current ripples are higher. To solve these problems, M. B. R. Corrê proposed the four-leg inverter [26]. Through suitable controlling the additional leg, its voltage utilization can be preserved. And then, S. Bolognani designed an innovative open-phase fault remedial scheme [8], [9]. This kind of remedial strategy is realized by compensating the unbalanced voltage. It is easy to operate and does not need reconfiguration of dq-axes current controllers after fault. However, when the ambient temperature or working condition varies in large scale, the change of the motor parameters (inductance and resistance) may lead to the degradation of the compensation effect.

The above open-phase PMSM fault-tolerance methods [8]–[25] have advantages such as simple or torque smooth. However, there are some disadvantages as follows:

(1) The tracking performances of sinusoidal current commands are unsatisfactory, such as hysteresis controller and resonant controller in [10], [11], [19].
(2) The robustness needs to be improved, such as the voltage feedforward compensation method in [8], [9].
(3) Applicability should be popularized, and complexity needs to be reduced, such as the motor modeling and field-oriented control method proposed in [17].

Then, a new open-phase fault tolerance method is proposed based on frame transformation [27], [28]. Through the new frame transformation, the modified sinusoidal current commands are transformed to dc variables. It is realized on the four-leg inverter and easy to operate. However, design of the additional inductance that is inserted in the neutral wire has not been explained. It should be noticed that the PMSM neutral wire inductance is typically very small. As a result, when the fourth leg is modulating, the neutral current ripple at usual switching frequencies may be very high. Therefore, an additional inductance should be added into the neutral wire [9]. It can be found that, the value of the additional inductance is very important which influences the coupling between phase voltage and current in the system equation, and affects the voltage limit ellipses simultaneously [9], [10]. Although most of the PMSM open-phase fault-tolerance methods are designed based on the four-leg inverter [19]–[23], however, the design theory of the additional inductance is rarely discussed in the existing literatures, further studies are still necessary.

To solve the above problem, a new open-phase PMSM fault-tolerance strategy is designed in this paper. Through the proposed frame transformation, the modified sinusoidal current commands of the remained phases are turned into dc variables in the redefined synchronous rotating frame. Thus, the design of the open-phase PMSM current controller can be simplified. This method can deal with different phase open faults (phases A, B, or C) and different current control modes ($i_d = 0$ or $i_d \neq 0$ mode). Furthermore, to eliminate the current ripple and obtain a suitable voltage limit ellipse, an optimal additional inductance is designed. With the designed additional inductance, complete decoupling can be achieved and the stronger nonlinear induced by the unbalanced three-phase windings can be eliminated. In addition, a comparison between the ELSC topology and ELES topology is conducted. It is verified that proposed open-phase PMSM fault-tolerance method has superior performance.

II. OPEN-PHASE PMSM FAULT TOLERACE METHOD

A. OPEN-PHASE MOTOR CURRENT COMMANDS

PMSM drive topology is displayed in Fig. 1, in which the neutral wire is available. Under healthy condition, traditional three-leg inverter and Clarke/Park transformation are employed, and the neutral point is not connected (Fig. 1(a)). If power switch fault occurs, the fault leg is replaced by the fourth leg directly (Fig. 1(b)). When open-phase fault presents in motor winding, the fault tolerance ability can be achieved through connecting the neutral point "n" to the

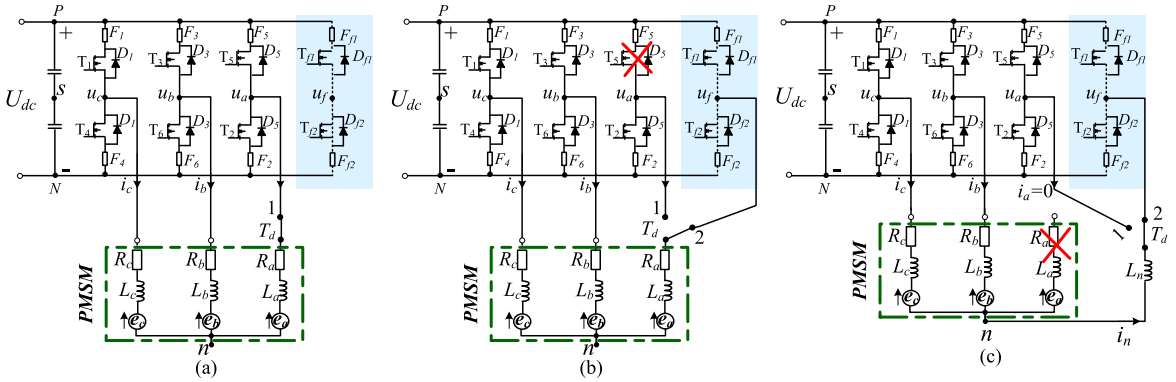

FIGURE 1. PMSM drive topology under different conditions.

TABLE 1. Modified current commands under different phase open-faults.

Fault phase	Modified current commands		
Phase A	$i_b^* = \sqrt{3}[i_d^* \sin(\theta - \frac{\pi}{3}) + i_q^* \cos(\theta - \frac{\pi}{3})]$,	$i_c^* = \sqrt{3}[i_d^* \sin(\theta - \frac{2\pi}{3}) + i_q^* \cos(\theta - \frac{2\pi}{3})]$,	$i_n^* = 3[i_d^* \sin(\theta - \frac{\pi}{2}) + i_q^* \cos(\theta - \frac{\pi}{2})]$
Phase B	$i_a^* = \sqrt{3}[i_d^* \sin(\theta + \frac{2\pi}{3}) + i_q^* \cos(\theta + \frac{2\pi}{3})]$,	$i_c^* = \sqrt{3}[i_d^* \sin(\theta + \pi) + i_q^* \cos(\theta + \pi)]$,	$i_n^* = 3[i_d^* \sin(\theta + \frac{5\pi}{6}) + i_q^* \cos(\theta + \frac{5\pi}{6})]$
Phase C	$i_a^* = \sqrt{3}[i_d^* \sin(\theta + \frac{\pi}{3}) + i_q^* \cos(\theta + \frac{\pi}{3})]$,	$i_b^* = \sqrt{3}[i_d^* \sin(\theta) + i_q^* \cos(\theta)]$,	$i_n^* = 3[i_d^* \sin(\theta + \frac{\pi}{6}) + i_q^* \cos(\theta + \frac{\pi}{6})]$

fourth leg (Fig. 1(c)). The switch symbol "T_d" in Fig. 1 is used for presenting bidirectional thyristor.

First, the expected phase current commands of the open-phase PMSM are analyzed in A-B-C reference frame to maintain the same torque. Assuming that phase A is disconnected, at this instant $i_a = 0$. Thus, $i_0 = -i_\alpha$ should be applied to the following Clarke inverse transformation,

$$\begin{bmatrix} i_a \\ i_b \\ i_c \end{bmatrix} = \begin{bmatrix} 1 & 0 & 1 \\ -1/2 & \sqrt{3}/2 & 1 \\ -1/2 & -\sqrt{3}/2 & 1 \end{bmatrix} \begin{bmatrix} i_\alpha \\ i_\beta \\ i_0 \end{bmatrix} \tag{1}$$

where, i_a, i_b, i_c are motor three-phase currents, i_α, i_β, i_0 are motor currents in α-β-0 coordinate, respectively. i_0 is zero-sequence current, $i_0 = i_n/3 = (i_a + i_b + i_c)/3$, which is null under normal condition.

By setting $i_0 = -i_\alpha$ in Eq.(1), the two current commands of the remained phases can be calculated,

$$\begin{cases} i_b^* = -\dfrac{3}{2} i_\alpha^* + \dfrac{\sqrt{3}}{2} i_\beta^* \\ i_c^* = -\dfrac{3}{2} i_\alpha^* - \dfrac{\sqrt{3}}{2} i_\beta^* \end{cases} \tag{2}$$

where, superscript '$*$' denotes command quantities.

According to the Park inverse transformation, the current commands i_α^* and i_β^* can be obtained from the corresponding current commands i_d^* and i_q^*,

$$\begin{cases} i_\alpha^* = i_d^* \cos\theta - i_q^* \sin\theta \\ i_\beta^* = i_d^* \sin\theta + i_q^* \cos\theta \end{cases} \tag{3}$$

where, i_d^* and i_q^* are the dq-axes current commands respect to the expected torque.

Substituting Eq.(3) into Eq.(2), the current commands in A-B-C reference frame can be obtained [8], [9] (shown in the first line of Table 1). Similarly, the corresponding current commands in the case of phases B and C faults can be obtained as described in the second and third lines of Table 1.

A concise current commands expression under different phase open faults can be written as,

$$\begin{cases} i_x^* = \sqrt{3} i_d^* \sin(\theta - \pi/3 + 2k\pi/3) + \sqrt{3} i_q^* \\ \cos(\theta - \pi/3 + 2k\pi/3) \\ i_y^* = \sqrt{3} i_d^* \sin(\theta - 2\pi/3 + 2k\pi/3) + \sqrt{3} i_q^* \\ \cos(\theta - 2\pi/3 + 2k\pi/3) \\ i_z^* = 0 \\ i_n^* = 3(i_d^* \sin(\theta - \pi/2 + 2k\pi/3) + i_q^* \\ \cos(\theta - \pi/2 + 2k\pi/3)) \end{cases} \tag{4}$$

where, subscripts x and y denote the remaining phases, subscript z denotes the open-phase, k is phase adjustment coefficient. When $z = a$, then $x = b$, $y = c$, $k = 0$; while $z = b$, then $x = c$, $y = a$, $k = 2$; If $z = c$, then $x = a$, $y = b$, $k = 1$.

For the normal PMSM, its dq-axes current commands can be described as Eq.(5) [29], [30],

$$\begin{cases} i_d^* = -I_s^* \sin\gamma \\ i_q^* = I_s^* \cos\gamma \end{cases} \tag{5}$$

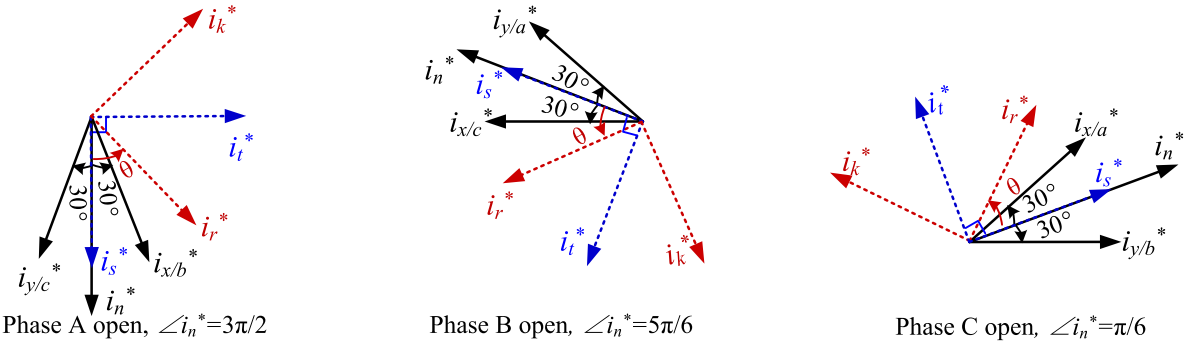

FIGURE 2. Healthy phase and neutral current commands under different phase faults.

where, I_s^* is current command amplitude, and γ is current angle, which denotes the angle between the sum vector of the three phase currents and the d-axis of the rotor, respectively. When $\gamma = 0$, $i_d = 0$ control mode is set.

Substituting Eq.(5) into Eq.(4), the remaining phase current commands can be rewritten as,

$$\begin{cases} i_x^* = -\sqrt{3}I_s^* \sin\gamma \sin(\theta - \pi/3 + 2k\pi/3) \\ +\sqrt{3}I_s^* \cos\gamma \cos(\theta - \pi/3 + 2k\pi/3) \\ i_y^* = -\sqrt{3}I_s^* \sin\gamma \sin(\theta - 2\pi/3 + 2k\pi/3) \\ +\sqrt{3}I_s^* \cos\gamma \cos(\theta - 2\pi/3 + 2k\pi/3) \\ i_n^* = 3(-I_s^* \sin\gamma \sin(\theta - \pi/2 + 2k\pi/3) \\ +I_s^* \cos\gamma \cos(\theta - \pi/2 + 2k\pi/3)) \end{cases} \tag{6}$$

As phase z is open, $i_z^* = 0$. It is neglected in Eq.(6). Through trigonometric function transformation, the modified current commands in Eq.(6) can be rewritten as

$$\begin{cases} i_x^* = \sqrt{3}I_s^* \cos(\theta + \gamma - \pi/3 + 2k\pi/3) \\ i_y^* = \sqrt{3}I_s^* \cos(\theta + \gamma - 2\pi/3 + 2k\pi/3) \\ i_n^* = 3I_s^* \cos(\theta + \gamma - \pi/2 + 2k\pi/3) \end{cases} \tag{7}$$

where, $\theta = \omega t$, ω is rotor angular velocity.

B. NEW REFERENCE FRAME TRANSFORMATION

It can be seen from Eq.(7) the modified current commands are synchronous with rotor flux. Assuming that $\gamma = 0$, the phase relationships among the modified current commands can be described in Fig. 2. For other current angle γ, the analysis is the same. In Fig. 2 the currents i_s^*, i_t^*, and i_r^*, i_k^* are the current commands in s-t frame and r-k frame, respectively.

According to the phase relationship described in Fig. 2, a stationary orthogonal coordinate transformation can be conducted first, similar to A-B-C frame → α-β frame transformation. In case of phase A open, the coordinate transformation from B-C-N frame to s-t frame can be obtained,

$$\begin{bmatrix} i_s^* \\ i_t^* \end{bmatrix} = T \cdot \begin{bmatrix} i_b^* \\ i_c^* \\ i_n^* \end{bmatrix} = \begin{bmatrix} \sqrt{3}/2 & \sqrt{3}/2 & 1 \\ 1/2 & -1/2 & 0 \end{bmatrix} \begin{bmatrix} i_b^* \\ i_c^* \\ i_n^* \end{bmatrix} \tag{8}$$

where matrix T = [$\sqrt{3}/2$ $\sqrt{3}/2$ 1; 1/2 −1/2 0], respectively.

As $i_n^* = i_b^* + i_c^*$, the matrix T in Eq.(8) can be simplified as a 2×2 matrix,

$$\begin{bmatrix} i_s^* \\ i_t^* \end{bmatrix} = T \cdot \begin{bmatrix} i_b^* \\ i_c^* \end{bmatrix} = \begin{bmatrix} (\sqrt{3}+2)/2 & (\sqrt{3}+2)/2 \\ 1/2 & -1/2 \end{bmatrix} \begin{bmatrix} i_b^* \\ i_c^* \end{bmatrix} \tag{9}$$

Then, the stationary s-t orthogonal frame is transformed to synchronous rotating r-k frame (as shown in Fig. 2). To remove the sinusoidal terms in the modified current commands, a special frame transformation is designed,

$$\begin{bmatrix} i_r^* \\ i_k^* \end{bmatrix} = [S \cdot T]_a \cdot \begin{bmatrix} i_b^* \\ i_c^* \end{bmatrix} = \begin{bmatrix} a\cos\theta & b\sin\theta \\ c\sin\theta & d\cos\theta \end{bmatrix} \cdot T \cdot \begin{bmatrix} i_b^* \\ i_c^* \end{bmatrix} \tag{10}$$

where S = [a·cosθ b·sinθ; c·sinθ d·cosθ], respectively.

Substituting the expression of i_x^* (i_b^*) and i_y^* (i_c^*) in Eq.(7) into Eq.(10), it can be derived that

$$\begin{bmatrix} i_r^* \\ i_k^* \end{bmatrix} = \sqrt{3}\, I_s^* \cdot \begin{bmatrix} k_1 \sin\gamma + k_2 & \sin(\gamma + 2\theta) \\ k_3 \cos\gamma + k_4 & \cos(\gamma + 2\theta) \end{bmatrix} \tag{11}$$

where k_1 = [(3+2$\sqrt{3}$)a − b]/4, k_2 =[(3+2$\sqrt{3}$)a + b]/4, k_3 = [(3+2$\sqrt{3}$)c+d]/4, k_4 = [(3+2$\sqrt{3}$)c−d]/4, respectively.

To simplify the current controller design, it is desired to make $i_r^* = i_d^*$, and $i_k^* = i_q^*$. Based on this idea, the parameters in the transformation matrix S can be obtained,

$$a = -2/(3\sqrt{3}+6),\ b = 2/\sqrt{3},\ c = 2/(3\sqrt{3}+6),\ d = 2/\sqrt{3} \tag{12}$$

Thus, the transformation from stationary B-C-N frame to synchronously rotating r-k frame can be expressed as

$$\begin{bmatrix} i_r^* \\ i_k^* \end{bmatrix} = [S \cdot T]_a \cdot \begin{bmatrix} i_b^* \\ i_c^* \end{bmatrix} = \begin{bmatrix} i_d^* \\ i_q^* \end{bmatrix} \tag{13}$$

where transformation matrix [S·T]$_a$ = 2/3[sin(θ − π/6) −sin(θ + π/6); sin(θ + π/3) sin(θ − π/3)].

The new dc commands i_r^*, i_k^*, which equal to i_d^*, i_q^* respectively, can be obtained with the transformation matrix [S·T]$_a$ under phase A open fault. However, when phase B or phase C open faults, the dc current commands cannot be obtained by designing the parameters a, b, c, d in Eq.(10).

To acquire the transformation matrixes in cases of phase B or phase C open, the relationship between the modified current commands under different phase faults should be analyzed. From Fig. 2 it can be seen that the phase differences between the opposite current commands under phase A, B and C open faults are $4\pi/3$ and $2\pi/3$, respectively. Hence, by conducting Euler rotation for the matrix $[\mathrm{S{\cdot}T}]_a$ (left multiplication), similar synchronous frame transformation can be performed under phase B and phase C open faults as shown in Eq.(14) and Eq.(15).

$$\begin{aligned}\begin{bmatrix} i_{\mathrm{r}}^* \\ i_k^* \end{bmatrix} &= \frac{2}{3}\begin{bmatrix} \cos(\frac{4\pi}{3}) & \sin(\frac{4\pi}{3}) \\ -\sin(\frac{4\pi}{3}) & \cos(\frac{4\pi}{3}) \end{bmatrix} \cdot [S\cdot T]_a \cdot \begin{bmatrix} i_c^* \\ i_a^* \end{bmatrix} \\ &= [S\cdot T]_b \cdot \begin{bmatrix} i_c^* \\ i_a^* \end{bmatrix} \end{aligned} \tag{14}$$

$$\begin{aligned}\begin{bmatrix} i_{\mathrm{r}}^* \\ i_k^* \end{bmatrix} &= \frac{2}{3}\begin{bmatrix} \cos(\frac{2\pi}{3}) & \sin(\frac{2\pi}{3}) \\ -\sin(\frac{2\pi}{3}) & \cos(\frac{2\pi}{3}) \end{bmatrix} \cdot [S\cdot T]_a \cdot \begin{bmatrix} i_a^* \\ i_b^* \end{bmatrix} \\ &= [S\cdot T]_c \cdot \begin{bmatrix} i_a^* \\ i_b^* \end{bmatrix} \end{aligned} \tag{15}$$

where, $[\mathrm{S{\cdot}T}]_b = 2/3[\cos(\theta+2\pi/3)\cos\theta; \sin(\theta-\pi/3) -\sin\theta]$, $[\mathrm{S{\cdot}T}]_c = 2/3[\cos\theta\ \sin(\theta-\pi/6); -\sin\theta\ \sin(\theta+\pi/3)]$, respectively.

And then, the reference frame transformation matrixes in cases of different phase open faults can be expressed as a general form as shown in Eq.(16).

$$\begin{bmatrix} i_{\mathrm{r}}^* \\ i_k^* \end{bmatrix} = [S\cdot T]_x \cdot \begin{bmatrix} i_x^* \\ i_y^* \end{bmatrix} = \begin{bmatrix} i_{\mathrm{d}}^* \\ i_q^* \end{bmatrix} \tag{16}$$

where, $[\mathrm{S{\cdot}T}]_x = 2/3[\sin(\theta-\pi/6+2k\pi/3)\ \sin(\theta+\pi/6+2k\pi/3);\ \sin(\theta+\pi/3+2k\pi/3)\ \sin(\theta-\pi/3+2k\pi/3)]$. The definitions of parameters k, x, y are consistent with the corresponding definitions in Eq.(4). With the new frame transformation, modified sinusoidal current commands are turned into dc variables ($i_r^* = i_d^*$, and $i_k^* = i_q^*$). Thus, the rated torque can be preserved, and the current controllers maintain unchanged after fault.

After open-phase fault, to drive the four-leg inverter the voltage control efforts u_r^*, u_k^* (r-k current controllers' outputs) should be transformed to u_{an}^*, u_{bn}^*, u_{cn}^*, u_{ns}^* in A-B-C-N frame. By inversing the transformation matrix $[\mathrm{S{\cdot}T}]_x$, the modified voltage efforts can be obtained,

$$\begin{bmatrix} u_{xn}^* \\ u_{yn}^* \end{bmatrix} = [S\cdot T]_x^{-1} \begin{bmatrix} u_r^* \\ u_k^* \end{bmatrix} \tag{17}$$

where, u_r^*, u_k^* are the voltage control efforts given by r-k current controllers under open-phase condition, u_{xn}^*, u_{yn}^* are the remaining phase voltage control efforts in A-B-C-N frame, $[\mathrm{S{\cdot}T}]_x^{-1} = 2/3[\sin(\theta-\pi/3+2k\pi/3)\ \sin(\theta+\pi/6+2k\pi/3);\ -\sin(\theta+\pi/3+2k\pi/3)\ \sin(\theta-\pi/6+2k\pi/3)]$, respectively.

And then, the voltage commands given to the PWM generator can be acquired [31]–[33],

$$\begin{cases} u_{ns}^* = -(\max(u_{bn}^*, u_{cn}^*) + \min(u_{bn}^*, u_{cn}^*))/2 \\ u_{xs}^* = u_{xn}^* + u_{ns}^* \\ u_{ys}^* = u_{yn}^* + u_{ns}^* \end{cases} \tag{18}$$

where, u_{xs}^*, u_{ys}^* are the voltage commands of motor terminal to dc-link midpoint, and u_{ns}^* is neutral point voltage command, respectively. It is worth to note that the power switches with respect to the open-phase are turned-off.

C. DETERMINATION OF THE ADDITIONAL INDUCTANCE L_N

Generally, an additional inductance L_n is inserted along the neutral wiring (see Fig. 1(c)). Noticed that the larger additional inductance would influence the voltage limit ellipses, while the smaller additional inductance cannot eliminate the current ripple. Hence, it is very important to determine the value of additional inductance L_n.

Assuming that phase A is opened and the influence of leakage inductance can be neglected, the motor voltage equation can be expressed as Eq. (19),

$$\begin{cases} u_{bf} = ri_b + L\dfrac{di_b}{dt} + M_{bc}i_c + e_b + r_n i_n + L_n\dfrac{di_n}{dt} \\ u_{cf} = ri_c + L\dfrac{di_c}{dt} + M_{bc}i_b + e_c + r_n i_n + L_n\dfrac{di_n}{dt} \end{cases} \tag{19}$$

where, u_{bf} and u_{cf} are the terminal voltage differences between the terminal voltages u_b and u_f, u_c and u_f, r and L are the winding phase resistance and self-inductance, r_n and L_n are the neutral wire resistance and inductance, M_{bc} is the mutual inductance between phase B and phase C, and $M_{bc} = -L/2$, e_b and e_c are the back-EMFs of phases B and C, respectively.

Eq.(19) can be rewritten as

$$\begin{aligned}\begin{bmatrix} u_{bf} \\ u_{cf} \end{bmatrix} &= \begin{bmatrix} r+r_n & r_n \\ r_n & r+r_n \end{bmatrix}\begin{bmatrix} i_b \\ i_c \end{bmatrix} \\ &\quad + \begin{bmatrix} L+L_n & L_n - L/2 \\ L_n - L/2 & L+L_n \end{bmatrix} p\begin{bmatrix} i_b \\ i_c \end{bmatrix} + \begin{bmatrix} e_b \\ e_c \end{bmatrix} \end{aligned} \tag{20}$$

where p is differential operator.

With the transformation matrix $[\mathrm{S{\cdot}T}]_a$, the voltage equation can be transformed to the r-k reference frame, as shown in Eq.(23), as shown at the bottom of the next page, where $u_{rk} = [u_r\ u_k]^{\mathrm{T}}$, $i_{rk} = [i_r\ i_k]^{\mathrm{T}}$, in which i_r, i_k, and u_r, u_k are motor current vector and voltage vector in r-k coordinates after the fault, respectively.

Substituting the expression of $[\mathrm{S{\cdot}T}]_a$ into Eq.(23), Eq.(23) can be rewritten as Eq.(24), as shown at the bottom of the next page, where $k_1 = -1-\cos2\theta/2$, $k_2 = -\sin2\theta/2$, $k_3 = -2\sin2\theta/\sqrt{3}+\cos2\theta$, $k_4 = 2\cos2\theta/\sqrt{3}-\sin2\theta$, $k_5 = \sin2\theta$, $k_6 = -2\sin2\theta/\sqrt{3}+1$, $k_7 = -2\sin2\theta/\sqrt{3}-\cos2\theta$, respectively.

Usually, $r_n << r$. Hence, r_n can be neglected in Eq.(24). In addition, it can be found that when $L_n = L/2$, Eq.(24) can be simplified as,

$$u_{rk} = \begin{bmatrix} r & 0 \\ 0 & r \end{bmatrix} i_{rk} + \begin{bmatrix} L_d & 0 \\ 0 & L_q \end{bmatrix} p i_{rk} + \omega \begin{bmatrix} 0 & -L_q \\ L_d & 0 \end{bmatrix} i_{rk} + \omega \psi_m \begin{bmatrix} k_1 \\ k_2 \end{bmatrix} \quad (21)$$

While the voltage equation of the healthy PMSM can be expressed as,

$$u_{dq} = \begin{bmatrix} r & 0 \\ 0 & r \end{bmatrix} i_{dq} + \begin{bmatrix} L_d & 0 \\ 0 & L_q \end{bmatrix} p i_{dq} + \omega \begin{bmatrix} 0 & -L_q \\ L_d & 0 \end{bmatrix} i_{dq} + \omega \psi_m \begin{bmatrix} 0 \\ 1 \end{bmatrix} \quad (22)$$

Compared Eq.(21) with Eq.(22), it can be seen that the main difference between the two voltage equations is the last term. Both the two last terms relate with motor speed (ω), which change slowly compared with the electrical variables such as winding current or phase voltage. Therefore, these two terms can be regarded as interference and can be eliminated by feedforward control if necessary. As for the cross couple terms ($\omega \cdot L_{dq} \cdot i_{dq,}$, the third term), it exist in the voltage equations pre- and post-fault. This term can be removed by decoupling and feedforward compensation, similar to the treatment in the healthy PMSM. For the interior PM motor, its self-inductance would change with magnetic saturation, working temperature. Under this condition, the additional inductance should be set as the average value of the self-inductance during normal operation. Although error may be induced, its influence is small which can be neglected (L_n-$L/2$ is a small aqueous). Therefore, by setting $L_n = L/2$ the open-phase PMSM almost has the same model as healthy PMSM. With simple PI controller, motor performance can be preserved.

D. COMPARISON BETWEEN ELSC TOPOLOGY AND ELES TOPOLOGY

1) VOLTAGE UTILIZATION

For the ELSC topology (employed in [17]), the neutral wire is connected to the middle point of the dc bus capacitor (point 's' in Fig. 1). Suppose that phase A is disconnected,

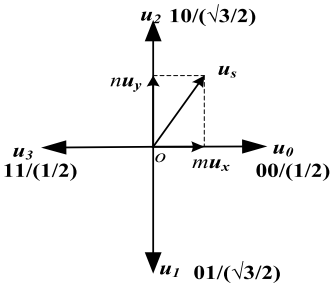

FIGURE 3. Schematic diagram of composited voltage vector.

motor terminal voltages can be expressed as

$$\begin{cases} u_b = U_{dc} \cdot S_b \\ u_c = U_{dc} \cdot S_c \\ u_n = U_{dc}/2 \end{cases} \quad (25)$$

where, u_b, u_c are motor terminal to ground voltages, u_n is neutral point to ground voltage, U_{dc} is the dc source voltage, and S_b and S_c are the switching signals corresponding to phases B and C, respectively.

The voltage drops on the phase winding can be written as

$$\begin{cases} u_{bn} = u_b - u_n \\ u_{cn} = u_c - u_n \end{cases} \quad (26)$$

and the composited voltage vector yielded by the phase voltages can be expressed as

$$\vec{u}_s = \vec{u}_{bn} + \vec{u}_{cn} = \vec{u}_\alpha + \vec{u}_\beta \quad (27)$$

where, $\vec{u}_s$ is the composited voltage vector, $\vec{u}_{bn}$ and $\vec{u}_{cn}$ are phase voltage vectors in A-B-C frame, $\vec{u}_\alpha$ and $\vec{u}_\beta$ are voltage vectors in α-β frame, respectively.

By controlling the switching signals S_b and S_c, 4 basic composited voltage vectors $\boldsymbol{u_0}$, $\boldsymbol{u_1}$, $\boldsymbol{u_2}$, $\boldsymbol{u_3}$ can be obtained ($\boldsymbol{u_0} = \frac{1}{2}e^{j0}$, $\boldsymbol{u_1} = \frac{\sqrt{3}}{2}e^{j\frac{3\pi}{2}}$, $\boldsymbol{u_2} = \frac{\sqrt{3}}{2}e^{j\frac{\pi}{2}}$, $\boldsymbol{u_3} = \frac{1}{2}e^{j\pi}$), and the available voltage area can be described in α-β reference frame as shown in Fig. 3.

As shown in Fig. 3, any two adjacent basic voltage vectors are orthometric, and the composited voltage vectors $\boldsymbol{u_s}$ can be expressed by the linear combination of the two basic voltage vectors ($\boldsymbol{u_x}$, $\boldsymbol{u_y}$),

$$\vec{u}_s = m \cdot \vec{u}_x + n \cdot \vec{u}_y \quad (28)$$

$$u_{rk} = [S \cdot T]_a \cdot \begin{bmatrix} u_{bf} \\ u_{cf} \end{bmatrix} = [S \cdot T]_a \cdot \begin{bmatrix} r + r_n & r_n \\ r_n & r + r_n \end{bmatrix} \cdot [S \cdot T]_a^{-1} \cdot i_{rk} + [S \cdot T]_a \cdot \begin{bmatrix} L + L_n & L_n - L/2 \\ L_n & -L/2L + L_n \end{bmatrix} \cdot p \cdot [S \cdot T]_a^{-1} \cdot i_{rk} + [S \cdot T]_a \cdot \begin{bmatrix} e_b \\ e_c \end{bmatrix} \quad (23)$$

$$u_{rk} = \begin{bmatrix} r & 0 \\ 0 & r \end{bmatrix} i_{rk} + \begin{bmatrix} L_d & 0 \\ 0 & L_q \end{bmatrix} p i_{rk} + \omega \begin{bmatrix} 0 & -L_q \\ L_d & 0 \end{bmatrix} i_{rk} + \omega \psi_m \begin{bmatrix} k_1 \\ k_2 \end{bmatrix} + r_n \begin{bmatrix} k_3 & k_4 \\ k_5 & k_6 \end{bmatrix} i_{rk} + (L_n - \frac{L}{2}) \begin{bmatrix} k_3 & k_4 \\ k_5 & k_6 \end{bmatrix} p i_{rk} + \omega (L_n - \frac{L}{2}) \begin{bmatrix} -k_5 & k_7 \\ 3 + 2k_1 & \frac{-2}{\sqrt{3}} - k_2 \end{bmatrix} i_{rk} \quad (24)$$

where, subscripts x, $y = 1, 2, 3, 4$, m and n are modulation coefficients, which are determined by the duty cycle of S_b and S_c, respectively.

The modulus of composited voltage vectors$\boldsymbol{u_s}$ can be expressed as,

$$|u_s| = \sqrt{(m \cdot u_x)^2 + (n \cdot u_y)^2} \quad (0 \le m, n \le 1, m + n \le 1) \tag{29}$$

According to Eq.(28), the maximum of $|\boldsymbol{u_s}|$ can be calculated,

$$u_{s\max} = \frac{\sqrt{3}}{4} U_{dc} \tag{30}$$

where, u_{smax} is the maximum of $|\boldsymbol{u_s}|$.

Therefore, the voltage utilization (u_{smax}/U_{dc}) of the ELSC topology is $\sqrt{3}/4$. Similarly, voltage utilization of ELES topology (employed in this paper) can be derived as $\sqrt{3}/2$. ELES topology possesses higher voltage utilization compared with ELSC topology.

2) THE CURRENT/VOLTAGE RIPPLE

In ELSC topology, two split capacitors are used for providing circuit for neutral current (see reference [17]). The polarities of the currents that flow into the upper and lower capacitors are opposite. So, the voltage of the two split capacitors becomes asymmetry which invokes the neutral point voltage fluctuation. In addition, the two split capacitors are hard to be same. Hence, the phase voltage/current may be distorted, which would affect the performance of the control system.

As for the ELES topology (see Fig.1(c)), although the neutral point voltage is modulated, the influence caused by the modulation can be eliminated by setting $L_n = L/2$. So, the phase voltage/current ripple is smaller.

E. FAULT-TOLERANT CONTROLLER STRUCTURE

The control block diagrams of the proposed method and voltage feedforward compensation method are described in Fig. 4 and Fig. 5. In the fault-tolerance system, motor fault state and fault phase are given by the fault phase judgement module. Compared with the healthy system, the proposed fault-tolerance system has similar structure and complexity. The differences between them are the reference frame transformation matrix and the modulation method. The transformation matrix used in the healthy system is derived based on Clarke and Park transformation, while the transformation matrix used in the proposed fault-tolerance system is derived based on the new transformation. When the motor is healthy, traditional transformation matrix is employed. Once open-phase fault occurs, traditional transformation matrix is replaced by the new matrix. Besides, in the proposed system, carrier-based PWM method is used for modulating the control effort, which provides lower harmonic currents and higher available modulation index [31]–[33].

However, there is an additional feedforward compensation module in the voltage feedforward compensation

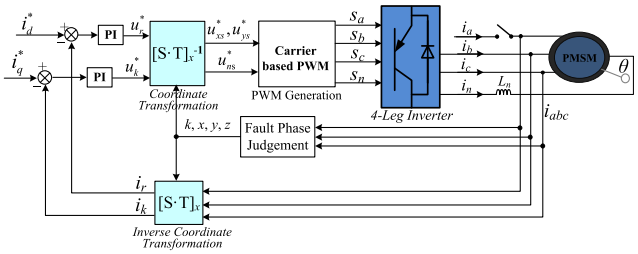

FIGURE 4. The control block diagrams of the proposed method.

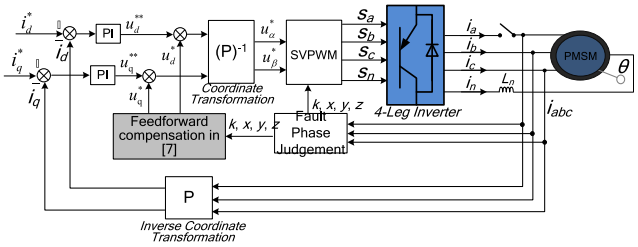

FIGURE 5. The control block diagrams of voltage feedforward compensation method.

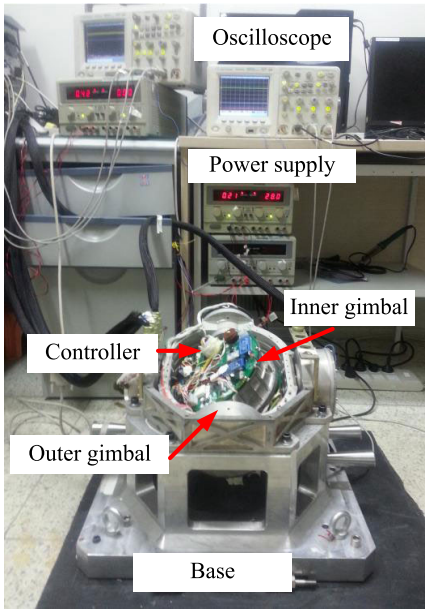

FIGURE 6. CMGs experimental system.

method [8], [9]. The feedforward voltage is calculated according to the difference between the dq-axes voltages applied to the remained phases (B, C, N) after fault and the voltages applied to the motor phase (A, B, C) before fault [8], [9]. As the parameters used in the feedforward compensation is fixed, its robustness is limited. Hence, compared with the healthy system and proposed system, this kind of fault-tolerance system is more complicated, and its robustness is poor.

It should be noticed that the open-phase PMSM is different from the two-phase PM motor with regard to motor design and control strategy. In the two-phase motor, there are two phase windings, and the phase difference between them

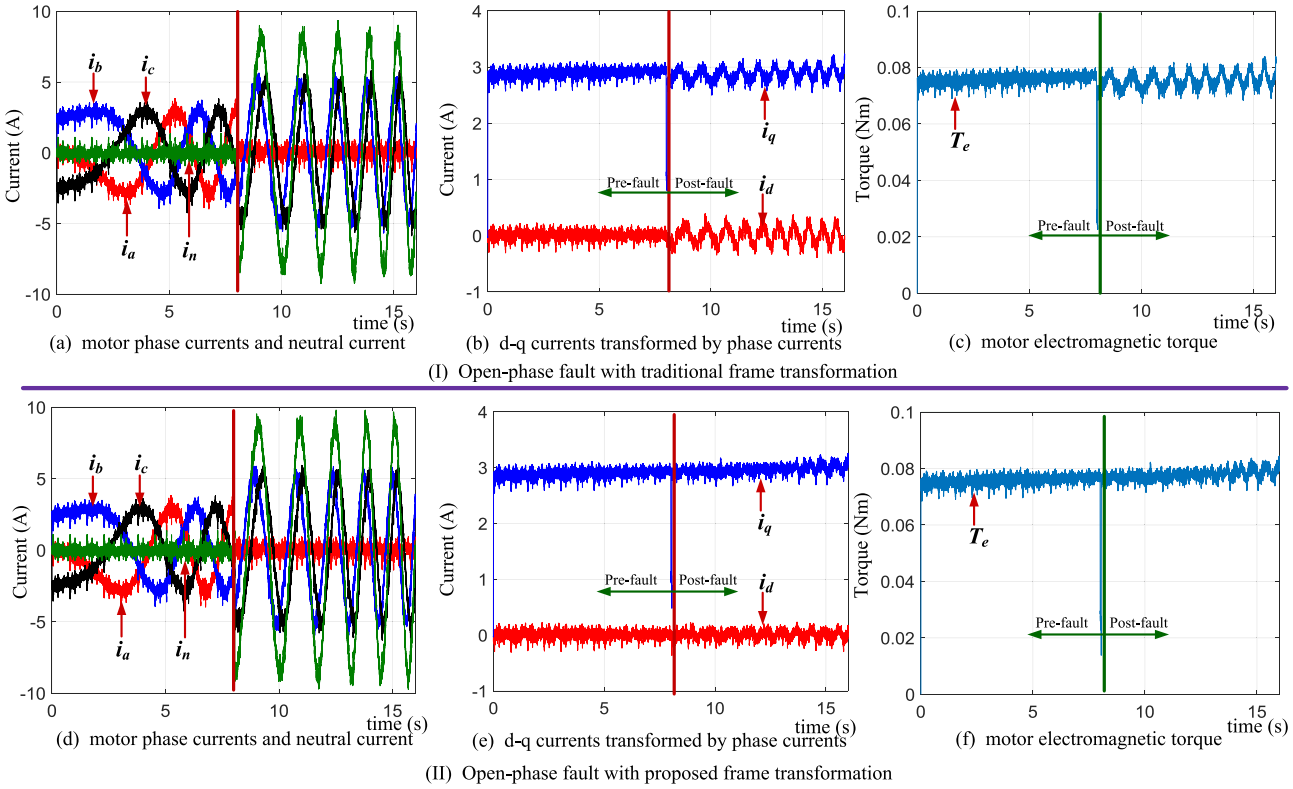

FIGURE 7. Comparison between traditional frame transformation and proposed transformation under motor open-phase fault.

is 90°. The dq-axes currents can be obtained by Park transformation without the use of Clarke transformation. Therefore, vector control can be employed directly. In the open-phase three-phase PMSM, the phase difference of the current in the two remained phases should be regulated to 60° to maintain the rated torque. Conventional Clarke and Park transformations can not be used for obtaining the orthorhombic dq-axes currents.

III. EXPERIMENTAL RESULTS

Control moment gyros (CMGs) prototype is utilized to evaluate the proposed fault tolerance method. Fig.6 shows the photograph of the CMGs platform. The CMGs gimbal is driven by PMSM. Key machine characteristics are listed in Table 2. For the experimental PMSM, additional inductance $L_n = 4.5$mH is chosen in the experiments.

The motor phase current is measured by high bandwidth hall effect current sensor and fed to the controller through 12-bit analog-to-digital (A/D) converter. The sampling frequency and switching frequency of the power switch is 20kHz, and the dead time is set as 200ns. As motor rated voltage and current are not very large, the influence caused by dead time can be neglected.

A. EXPERIMENT 1: COMPARISON BETWEEN TRADITIONAL AND PROPOSED FRAME TRANSFORMATIONS

In this experiment the current commands $I_s^* = 3$A, current angle $\gamma = 0$, and PI parameters $k_{dp} = 90$, $k_{di} = 6$, $k_{qp} = 90$, $k_{qi} = 6$ are set, where k_{dp}, k_{di}, k_{qp}, and k_{qi} are the proportional and integral coefficients of the dq-axes current PI controllers, respectively.

TABLE 2. CMGs gimbal motor characteristics.

DC power supply Udc (V)	48
Nominal current (A)	3
Nominal speed (rad/s)	2.5
Nominal power(W)	25
Permanent flux linkage (Vs/rad)	0.55
Pairs	4
Phase Resistance R (Ω)	6
Phase Inductance L (mH)	9
Angular momentum H (N·m·s)	10

First, the motor performance is tested under open-phase fault with traditional Clarke and Park frame transformation. Assuming that phase A is disconnected at t=8s, at this instant the current in phase A decreases to zero immediately, and the neutral wiring is connected to the fourth leg. Although the fourth leg provides circuit for the healthy phase currents, the yielded dq-axes currents present distinct fluctuations due to the unbalanced three-phase currents (see Fig. 7(I)).

Then, the proposed fault-tolerant method is employed in the system after fault occurrence. In the proposed method, the proposed frame transformation is applied, and same PI parameters are used in the current regulators under healthy and fault conditions. From Fig. 7 (II) it can be noted that

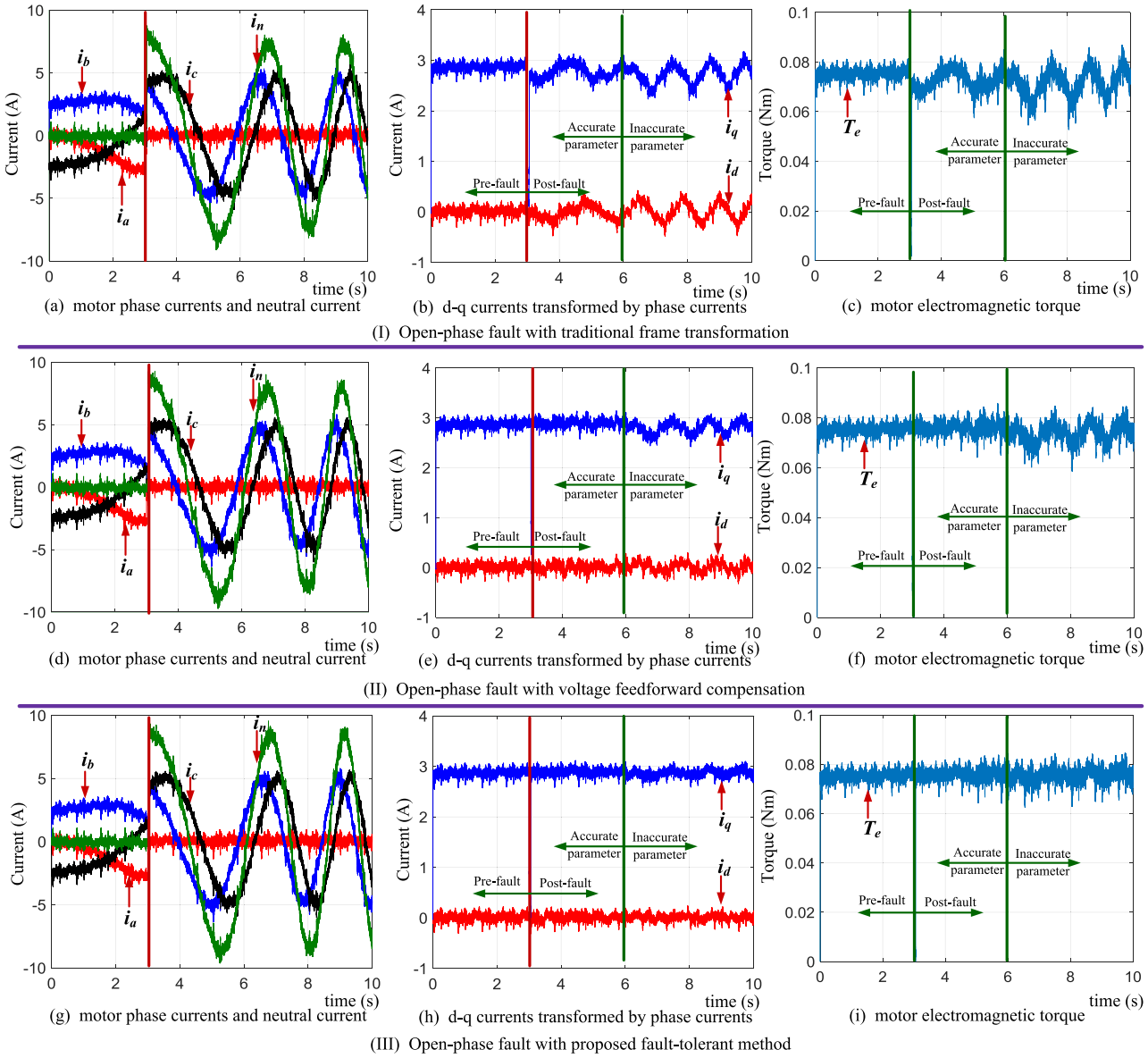

FIGURE 8. Performance comparison between different fault-tolerance method when motor parameters change.

the dq-axes current fluctuation reduces distinctly, which is almost the same as pre-fault state. Besides, the motor toque performance improves simultaneously.

B. EXPERIMENT 2: ROBUSTNESS TESTES BETWEEN DIFFERENCE METHODS

Considering that phase inductance is position dependent in 3-phase reference frame for IPM, its average value is used in this method. In practice, when the average value of phase inductance is chosen, the maximum inductance error in different position is less than 25%. In this experiment, the robustness of different methods is verified when motor parameters change. In the tests, open-phase fault occurs at t=3s and motor parameters change after t=6s. The phase resistance and additional inductance increase by 50% when t>6s. The increases of the resistance and inductance are realized by SPDT switch. With these settings, detailed experiments are made.

First, the traditional Clarke and Park transformation is applied to the system. When the open-phase fault occurs, the traditional frame still operates. From Fig. 8 (I) it can be seen that distinct current and torque fluctuations appear after motor winding fault, and these fluctuations are even larger when motor parameters changes.

Then, the voltage feedforward compensation method proposed in [8], [9] is applied to the system for fault tolerance. As shown in Fig. 8 (II), when motor parameters are accurate the current and torque fluctuations reduce distinctly compared with the system employing traditional frame transformation. However, when motor parameter changes,

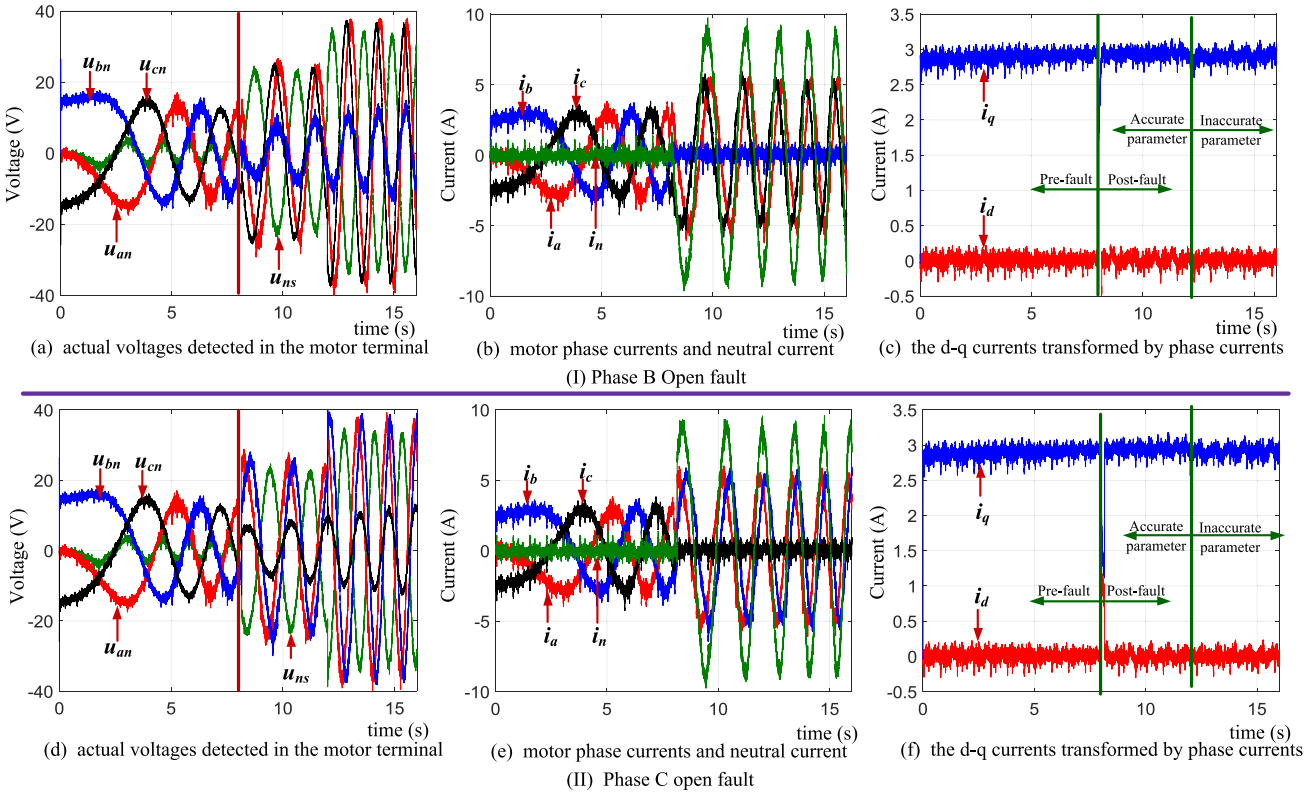

FIGURE 9. PMSM drive under different phase open faults.

the compensation effect degrades, and motor torque performance reduces obviously.

Then, the proposed open-phase fault-tolerance method is applied to the open-phase PMSM system. From Fig. 8 (III), we can observe that dq-axes currents performances improve obviously through the new frame transformation. Besides, it can be found that torque performance degrades indeed when motor inductance changes 50%. But, the dq-axes currents fluctuations are very small, which is acceptable. The experiment result indicates that the proposed method possesses superior robustness than other methods.

C. EXPERIMENT 3: DIFFERENT PHASE OPEN FAULT TOLERANCE

In this experiment, the performance of proposed fault-tolerant method is verified under different phase open faults.

The current command $I_s^* = 3$A, and current angle $\gamma = 0$ is set. As the open fault in phase A has been tested in experiment 1, this experiment just tests the performance of the proposed method under phase B and phase C open faults. The yielded terminal voltage, phase currents, and dq-axes currents are illustrated in Fig. 9 (I) and (II). To display at least one periods in the oscilloscope, the time axis should be set longer. Hence, the measured voltages look like sinusoidal not PWM style.

From Fig. 9 it can be observed that the neutral current is the sum of the two remained phase currents. With the proposed open-phase fault-tolerant method, the dq-axes currents performances can be preserved under different phase open faults. Particularly, with the proposed method the motor performance can be preserved even when the motor parameters change distinctly.

D. EXPERIMENT 3: PERFORMANCE TEST IN $I_D \neq 0$ Mode

In this experiment, phase C open fault under $i_d \neq 0$ mode is tested. At first, the current command is set as $I_s^* = 3$A and $\gamma = 0$. Phase C is opened at t = 10s, and then at t = 16s the current command changes to $I_s^* = 3$A and $\gamma = \pi/4$. Hence, before t = 16s, $i_d^* = 0$A, $i_q^* = 3$A, after t = 16s, $i_d^* = -2.12$A, $i_q^* = 2.12$A. With these settings, detailed experiment is conducted.

The motor voltage and current waveforms yielded by the proposed fault tolerance system are shown in Fig. 10. We can observe that the motor works well under normal condition. When the open-phase fault presents, the current in the fault phase reduces to zero immediately. While the current in the remained phase currents increase rapidly to compensate the change of dq-axes currents and torque. As reported in Fig. 10(b) the dq-axes currents are almost unchanged after the open-phase fault occurrence. In addition, when the current angle changes to $\gamma = \pi/4$ at t=16s, dq-axes currents change with the change of current commands at once (see Fig. 10(b)). The open-phase PMSM possesses superior performance no matter which kind of current control mode is adopted.

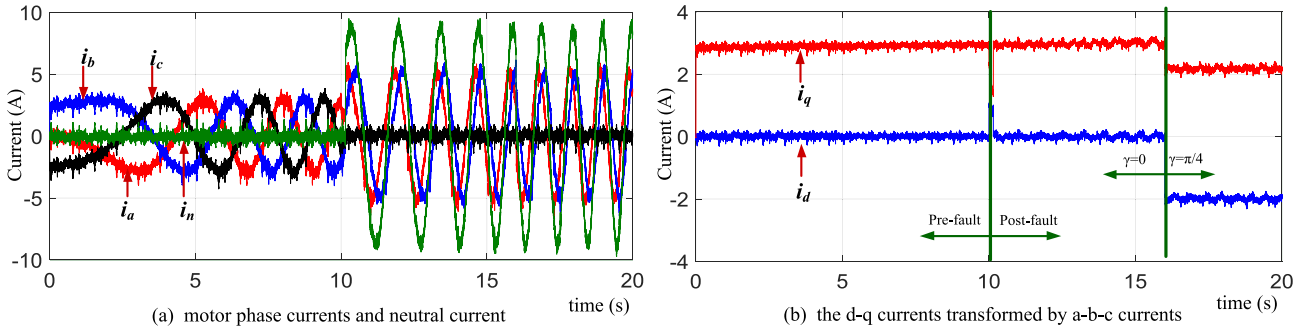

(a) motor phase currents and neutral current

(b) the d-q currents transformed by a-b-c currents

FIGURE 10. Proposed open-phase fault-tolerant method in $i_d \neq 0$ control mode.

Noticed that in all of the experiments, same PI controller is used, and its parameters are unchanged during pre- and post-fault operations.

IV. CONCLUSION

Open-phase fault may result in motor current/torque ripple and efficiency degradation. To improve PMSM post-fault performance, a general fault tolerance method for the open-phase PMSM is proposed in this paper. It is designed based on a novel reference frame transformation. Through proposed frame transformation, the modified sinusoidal time-varying current commands in the remained phases are turned into dc variables in the redefined synchronous rotating frame. Hence, the design of the open-phase PMSM current controller can be simplified. The proposed open-phase fault-tolerant method can deal with different phase open faults and different current control modes ($i_d = 0$ or $i_d \neq 0$ mode). Furthermore, to eliminate the current ripple and obtain a suitable voltage limit ellipse, the additional inductance inserted in the neutral wire is designed. With the designed additional inductance, complete decoupling can be achieved and the stronger nonlinear induced by the unbalanced three-phase windings can be eliminated. Finally, the effectiveness of the new open-phase PMSM fault tolerance method has been validated by sufficient experiments on the PMSM in CMGs.

REFERENCES

[1] Y. Wu, B. Jiang, and N. Lu, "A descriptor system approach for estimation of incipient faults with application to high-speed railway traction devices," *IEEE Trans. Syst., Man, Cybern. Syst.*, vol. 49, no. 10, pp. 2108–2118, Oct. 2019. doi: 10.1109/TSMC.2017.2757264.

[2] M. J. Duran and F. Barrero, "Recent advances in the design, modeling, and control of multiphase machines—Part II," *IEEE Trans. Ind. Electron.*, vol. 63, no. 1, pp. 459–468, Jan. 2016.

[3] H. S. Ro, D. H. Kim, H. G. Jeong, and K. B. Lee, "Tolerant control for power transistor faults in switched reluctance motor drives," *IEEE Trans. Ind. Appl.*, vol. 51, no. 4, pp. 3187–3197, Jul. 2015.

[4] H. S. Che, M. J. Duran, E. Levi, M. Jones, W.-P. Hew, and N. A. Rahim, "Postfault operation of an asymmetrical six-phase induction machine with single and two isolated neutral points," *IEEE Trans. Power Electron.*, vol. 29, no. 10, pp. 5406–5416, Oct. 2014.

[5] A. Tani, M. Mengoni, L. Zarri, G. Serra, and D. Casadei, "Control of multiphase induction motors with an odd number of phases under open-circuit phase faults," *IEEE Trans. Power Electron.*, vol. 27, no. 2, pp. 565–577, Feb. 2012.

[6] A. S. Abdel-Khalik, A. S. Morsy, S. Ahmed, and A. M. Massoud, "Effect of stator winding connection on performance of five-phase induction machines," *IEEE Trans. Ind. Electron.*, vol. 61, no. 1, pp. 3–19, Jan. 2014.

[7] F. Baudart, B. Dehez, E. Matagne, D. Telteu-Nedelcu, P. Alexandre, and F. Labrique, "Torque control strategy of polyphase permanent-magnet synchronous machines with minimal controller reconfiguration under open-circuit fault of one phase," *IEEE Trans. Ind. Electron.*, vol. 59, no. 6, pp. 2632–2644, Jun. 2012.

[8] S. Bolognani, M. Zordan, and M. Zigliotto, "Experimental fault-tolerant control of a PMSM drive," *IEEE Trans. Ind. Electron.*, vol. 47, no. 5, pp. 1134–1141, Oct. 2000.

[9] N. Bianchi, S. Bolognani, M. Zigliotto, and M. Zordan, "Innovative remedial strategies for inverter faults in IPM synchronous motor drives," *IEEE Trans. Energy Convers.*, vol. 18, no. 2, pp. 306–314, Jun. 2003.

[10] F. Meinguet and J. Gyselinck, "Control strategies and reconfiguration of four-leg inverter PMSM drives in case of single-phase open-circuit faults," in *Proc. IEEE Int. Electr. Mach. Drives Conf.*, May 2009, pp. 299–304.

[11] Z. Q. Zhu, K. Utaikaifa, K. Hoang, Y. Liu, and D. Howe, "Direct torque control of three-phase PM brushless AC motor with one phase open-circuit fault," in *Proc. IEEE Int. Electr. Mach. Drives Conf.*, May 2009, pp. 1180–1187.

[12] A. Kuperman, "Proportional-resonant current controllers design based on desired transient performance," *IEEE Trans. Power Electron.*, vol. 30, no. 10, pp. 5341–5345, Oct. 2015.

[13] A. G. Yepes, F. D. Freijedo, J. Doval-Gandoy, O. López, J. Malvar, and P. Fernandez-Comesaña, "Effects of discretization methods on the performance of resonant controllers," *IEEE Trans. Power Electron.*, vol. 25, no. 7, pp. 1692–1712, Jul. 2010.

[14] R. Bojoi, L. R. Limongi, F. Profumo, D. Roiu, and A. Tenconi, "Analysis of current controllers for active power filters using selective harmonic compensation schemes," *IEEJ Trans. Elect. Electron. Eng.*, vol. 4, no. 2, pp. 139–157, Mar. 2009.

[15] D. G. Holmes, T. A. Lipo, B. P. McGrath, and W. Y. Kong, "Optimized design of stationary frame three phase AC current regulators," *IEEE Trans. Power Electron.*, vol. 24, no. 11, pp. 2417–2426, Nov. 2009.

[16] M. C. Chou and C. M. Liaw, "Development of robust current 2-DOF controllers for a permanent magnet synchronous motor drive with reaction wheel load," *IEEE Trans. Power Electron.*, vol. 24, no. 5, pp. 1304–1320, May 2009.

[17] A. Gaeta, G. Scelba, and A. Consoli, "Modeling and control of three-phase PMSMs under open-phase fault," *IEEE Trans. Ind. Appl.*, vol. 49, no. 1, pp. 74–83, Jan./Feb. 2013.

[18] K. D. Hoang, Z. Q. Zhu, M. P. Foster, and D. A. Stone, "Comparative study of current vector control performance of alternate fault tolerant inverter topologies for three-phase PM brushless ac machine with one phase open-circuit fault," in *Proc. 5th IET Int. Conf. Power Electron., Mach. Drives (PEMD)*, Apr. 2010, pp. 1–6.

[19] O. Jasim, M. Sumner, C. Gerada, and J. Arellano-Padilla, "Development of a new fault-tolerant induction motor control strategy using an enhanced equivalent circuit model," *IET Electr. Power Appl.*, vol. 5, no. 8, pp. 618–627, Sep. 2011.

[20] S. Khwan-on, L. D. Lillo, L. Empringham, P. Wheeler, and C. Gerada, "Fault-tolerant, matrix converter, permanent magnet synchronous motor drive for open-circuit failures," *IET Elect. Power Appl.*, vol. 5, no. 8, pp. 654–667, Sep. 2011.

[21] O. Wallmark, L. Harnefors, and O. Carlson, "Control algorithms for a fault-tolerant PMSM drive," *IEEE Trans. Ind. Electron.*, vol. 54, no. 4, pp. 1973–1980, Aug. 2007.
[22] F. Meinguet, E. Semail, and J. Gyselinck, "Enhanced control of a PMSM supplied by a four-leg voltage source inverter using the homopolar torque," in *Proc. 18th Int. Conf. Elect. Mach.*, Sep. 2008, pp. 1–6.
[23] W. Wang, J. Zhang, and M. Cheng, "Common model predictive control for permanent-magnet synchronous machine drives considering single-phase open-circuit fault," *IEEE Trans. Power Electron.*, vol. 32, no. 7, pp. 5862–5872, Jul. 2017.
[24] A. Gaeta, G. Scelba, and A. Consoli, "Sensorless vector control of PM synchronous motors during single-phase open-circuit faulted conditions," *IEEE Trans. Ind. Appl.*, vol. 48, no. 6, pp. 1968–1979, Nov./Dec. 2012.
[25] K. D. Hoang, Z. Q. Zhu, M. P. Foster, and D. A. Stone, "Comparative study of current vector control performance of alternate fault tolerant inverter topologies for three-phase PM brushless AC machine with one phase open-circuit fault," in *Proc. 5th IET Int. Conf. Power Electron., Mach. Drives (PEMD)*, Apr. 2010, pp. 1–6.
[26] M. B. D. R. Correa, C. B. Jacobina, E. R. C. D. Silva, and A. M. N. Lima, "An induction motor drive system with improved fault tolerance," *IEEE Trans. Ind. Appl.*, vol. 37, no. 3, pp. 873–879, May 2001.
[27] X. Zhou, J. Sun, H. Li, and X. Song, "High performance three-phase PMSM open-phase fault-tolerant method based on reference frame transformation," *IEEE Trans. Ind. Electron.*, vol. 66, no. 10, pp. 7571–7580, Oct. 2019.
[28] X. Zhou, J. Sun, H. Li, M. Lu, and F. Zeng, "PMSM open-phase fault-tolerant control strategy based on four-leg inverter," *IEEE Trans. Power Electron.*, to be published. doi: 10.1109/TPEL.2019.2925823.
[29] F.-J. Lin, Y.-T. Liu, and W.-A. Yu, "Power perturbation based MTPA with an online tuning speed controller for an IPMSM drive system," *IEEE Trans. Ind. Electron.*, vol. 65, no. 5, pp. 3677–3687, May 2018.
[30] T. Sun, M. Koç, and J. Wang, "MTPA control of IPMSM drives based on virtual signal injection considering machine parameter variations," *IEEE Trans. Ind. Electron.*, vol. 65, no. 8, pp. 6089–6098, Aug. 2018.
[31] J.-H. Kim and S.-K. Sul, "A carrier-based PWM method for three-phase four-leg voltage source converters," *IEEE Trans. Power Electron.*, vol. 19, no. 1, pp. 66–75, Jan. 2004.
[32] J. H. Kim, S. K. Sul, and P. N. Enjeti, "A carrier-based PWM method with optimal switching sequence for a multilevel four-leg voltage-source inverter," *IEEE Trans. Ind. Appl.*, vol. 44, no. 4, pp. 1239–1248, Jul. 2008.
[33] Y. Kumsuwan, S. Premrudeepreechacharn, and V. Kinnares, "A carrier-based unbalanced PWM method for four-leg voltage source inverter fed unsymmetrical two-phase induction motor," *IEEE Trans. Ind. Electron.*, vol. 60, no. 5, pp. 2031–2041, May 2013.

XINXIU ZHOU (M'14) received the B.S. degree in motor drives and control and power electronic devices from Yanshan University, Hebei, China, in 2006, and the Ph.D. degree in the area of attitude control system technology of spacecraft and novel inertial instrument and equipment technology from Beihang University, Beijing, China, in 2013.

She is currently a Research Member with the Key Laboratory of Fundamental Science for National Defense, Novel Inertial Instrument and Navigation System Technology, Beijing. Her research interests include motor control, power electron, and spacecraft attitude control.

SHUN LI received the B.S. and M.S. degrees from the North China University of Technology, Beijing, China, in 2006 and 2010, respectively. He is currently pursuing the Ph.D. degree with the School of Instrumentation and Optoelectronic Engineering, Beijing University of Aeronautics and Astronautics, Beijing.

He is currently a Research Member with the Key Laboratory of Fundamental Science for National Defense, Novel Inertial Instrument and Navigation System Technology, Beijing. His research interests include the motor control and spacecraft attitude control.

MING LU received the B.S. and M.S. degrees from Xi'an Jiaotong University, in 2004 and 2007, respectively, and the Ph.D. degree from the Chinese Academy of Electrical Engineering, in 2013. He is currently a Senior Engineer with the Beijing Institute of Control Engineering. His main research interests include high precision space actuator, active magnetic bearing, and robust control.

FANQUAN ZENG received the B.S. degree from the Harbin Institute of Technology, Harbin, China, in 1997. He is currently a Senior Engineer with the Shanghai Servo System Engineering Technology Research Center and Servo Control Technology, and the Shanghai Institute of Spaceflight Control Technology.

His main research interests include thrust vector control systems, servo motor control, intelligent space robot control, and advanced control algorithms simulation.

MIN ZHU received the bachelor's degree in measurement and control technology and instruments from the University of Science and Technology in Beijing, Beijing, China, in 2012, and the master's degree in the area of attitude control system technology of spacecraft and novel inertial instrument and equipment technology from Beihang University, Beijing, in 2015.

She is currently an Engineer with the Shanghai Institute of Satellite Engineering. Her research interests include motor control, satellite system design, and spacecraft attitude control.

YANG YU received the B.S. and M.S. degrees from the Beijing University of Chemical Technology, China, in 2005 and 2008, respectively, and the Ph.D. degree from Beihang University, China in 2012. He is currently a Research Fellow with the Faulty of Engineering and Information Technology, University of Technology Sydney, Australia. His current research interests include data fusion, machine learning, and nonlinear modeling.